

First-principles study of the formation and migration of native defects in $\text{LiNH}_2\text{BH}_3^\dagger$

Cite this: *Phys. Chem. Chem. Phys.*, 2013, **15**, 893

Xiaowei Chen,^a Yu-Jun Zhao^b and Xuebin Yu^{*a}

First-principles calculations based on density functional theory were carried out to investigate the formation and migration of native defects in LiNH_2BH_3 . The structural properties and formation energies of H, Li, N and B related defects in various charge states were examined. Our analysis showed that the dominant atomic H defects are positively and negatively charged H interstitial (I_{H^+} and I_{H^-}). The Li related defects are dominated by positively charged Li interstitial (I_{Li^+}) and negatively charged Li vacancy (V_{Li^-}). For N related defects, the energetically favorable defects are positively and negatively charged NH_2 interstitial ($I_{\text{NH}_2^+}$ and $I_{\text{NH}_2^-}$), while B related defect is dominated by neutral BH_3 interstitial ($I_{\text{BH}_3^0}$). Further results indicated that the neutral H_2 interstitial (I_{H_2}) has the lowest formation energy (0.31 eV), suggesting that the major defect in LiNH_2BH_3 is I_{H_2} . Investigation of migration processes of the defects showed that the migration barriers for $V_{(\text{B})\text{H}^+}$ (positively charged H vacancy on a B–H site), I_{H^+} and I_{H^-} are relatively high (0.50–0.68 eV), whereas moderate diffusion barriers are presented for $V_{(\text{N})\text{H}^-}$ (negatively charged H vacancy on a N–H site) and I_{Li^+} (0.29 and 0.32 eV, respectively). The V_{Li^-} and I_{H_2} defects can migrate with low energy barriers of 0.13 and 0.16 eV, respectively. With a low activation energy of 0.47 eV, I_{H_2} is the major diffusive species in LiNH_2BH_3 . Our calculation results further suggest that the creation of the $V_{(\text{N})\text{H}^-}$, I_{Li^+} and V_{Li^-} defects is the rate-limiting step for their transportation in LiNH_2BH_3 .

Received 29th August 2012,
Accepted 16th November 2012

DOI: 10.1039/c2cp43016a

www.rsc.org/pccp

1 Introduction

Hydrogen is an ideal candidate as an energy carrier due to a series of advantages such as its high heating value per mass, and being regenerative and environmentally friendly. However, the lack of safe and efficient hydrogen storage technologies is one of the key barriers in developing hydrogen as a fuel for mobile and stationary applications.^{1,2} Recently, many efforts have been focused on chemical hydrides due to their high gravimetric energy density,^{1,3,4} among which ammonia borane is a promising candidate for hydrogen storage and has received disproportionately attention owing to its features of high gravimetric storage density (19.6 wt%), and non-flammability and non-explosivity under standard conditions.^{5–7} However, along with the dominant hydrogen evolution, the decomposition of ammonia borane also produces volatile byproducts,

e.g. ammonia and borazine, which not only reduce the hydrogen storage capacity but also poison the polymer electrolyte membrane of fuel cells. During the past decades, various attempts have been conducted to overcome the drawbacks of ammonia borane, of which one approach is to substitute one H atom in the NH_3 group by an alkali metal to form single or double metal amidoborane (MAB), *e.g.* LiNH_2BH_3 ,^{4,8,9} NaNH_2BH_3 ,^{4,9} $\text{Ca}(\text{NH}_2\text{BH}_3)_2$,^{10,11} $\text{Na}_2\text{Mg}(\text{NH}_2\text{BH}_3)_4$ ¹² and $\text{NaLi}(\text{NH}_2\text{BH}_3)_2$.¹³ These metal amidoborane compounds presented significantly improved dehydrogenation properties compared to AB in terms of the reduced dehydrogenation temperatures, accelerated H_2 release kinetics and/or minimized borazine release. For example, LiNH_2BH_3 is able to release a high storage capacity (10.9 wt%) of hydrogen at easily accessible dehydrogenation temperatures (about 90 °C) without the unwanted by-product borazine,⁴ thus enabling this material to be a promising candidate for hydrogen storage.

It is well known that crystal defects play an important role in chemical reactions and that their presence significantly affects the atomic diffusion and mass transport properties in materials.¹⁴ The transport properties of hydrogen are crucial to the kinetics of (de)hydrogenation in hydrogen storage materials. Therefore, the microscopic mechanisms behind the dehydrogenation of

^a Department of Materials Science, Fudan University, Shanghai, China 200433.
E-mail: yuxuebin@fudan.edu.cn; Tel: +86-21-5566 4581

^b Department of Physics, South China University of Technology, Guangzhou, China 510640

† Electronic supplementary information (ESI) available: Band structure for LiNH_2BH_3 , energy profiles and trajectories for the migration of selective defects. See DOI: 10.1039/c2cp43016a

hydrogen storage materials may relate to the formation and diffusivity of defects. Previous theoretical works have shown that H diffusion in NaAlH_4 ,^{15,16} MgH_2 ^{17,18} and LiNH_2 ^{19,20} are dominated by the existence of charged defects, while the mobility of H in solid borohydrides is dominated by neutral H_2 interstitial (I_{H_2}) rather than the charged defects,²¹ indicating the varied effect of defects on different hydrogen storage systems. The study of native defects in NH_3BH_3 suggested that the formation energies for the charge-neutral defects, depending on the growth conditions, can be surprisingly low. This can be understood in terms of the molecular nature of the NH_3BH_3 , which is made of the NH_3 and BH_3 molecular building blocks.²² Although several first-principles studies have been conducted on AB and MAB to determine the structures, decomposition pathways and energetics of H desorption during the past few years,^{23–29} it is rare that detailed theoretical studies by first-principles calculations have been devoted to the formation ability and diffusion processes of native defects in MAB. In this paper, we carried out detailed first-principles calculations on the formation energies and diffusion events of relevant native defects in LiNH_2BH_3 with various possible states. It is expected that this study may deepen the understanding of the fundamental properties of LiNH_2BH_3 , and provide useful clues for improving its dehydrogenation kinetics.

2 Computation method

The calculations are based on density-functional theory (DFT) within the generalized gradient approximation (GGA)³⁰ and the projector augmented wave (PAW) method³¹ as implemented in the VASP code.^{32,33} Plane waves with kinetic energy cutoff of 500 eV were used. The equilibrium lattice parameters of LiNH_2BH_3 were calculated using a $3 \times 2 \times 5$ Monkhorst-Pack k-point meshes.³⁴ For the calculation of point defects, to prevent the spurious interactions between neighboring defects in the supercell and get well-converged results, various sizes of supercells and k-points were examined. Tests showed the use of a $1 \times 1 \times 2$ supercell (contains 128 atoms) with a $4 \times 2 \times 2$ k-point mesh yields energies that converged within 0.01 eV/(f.u.). Vacancy (interstitial) was created by removing (adding) atoms from (to) the LiNH_2BH_3 supercell. For charged defects, a compensating background charge was included in order to prevent divergence of the total energy for a charged system. The geometry optimization was performed in fixed lattice constants while atomic positions in the supercell were allowed to fully relax until the residual forces were less than 0.03 eV \AA^{-1} .

The concentration of defects in the solid states could be determined by their formation energies by the following eqn (1).³⁵

$$c = N_{\text{sites}} N_{\text{config}} \exp(-E_f/kT) \quad (1)$$

where E_f is the formation energy; N_{sites} is the number of sites in which the defect can be incorporated; N_{config} is the number of configurations per site in which the defect can be formed; k is the Boltzmann constant, and T is the temperature.

The formation energies of intrinsic defects depend on the chemical potentials of Li, B, N and H, and also vary with the

electronic chemical potential (the Fermi level) if a defect has a charge of q . For a defect with the charge state of q , its formation energy (E_f) is given by eqn (2).³⁶

$$E_f(X^q) = E_{\text{tot}}(X^q) - E_{\text{tot}}(\text{bulk}) - \sum_i n_i \mu_i + q(\varepsilon_V + \varepsilon_F \Delta V) \quad (2)$$

where $E_{\text{tot}}(X^q)$ is the total energy of bulk with X defect in the charged state q ; $E_{\text{tot}}(\text{bulk})$ is the total energy of bulk without defect; μ_i is the chemical potential of species i ; n_i is the atoms of species i being added to ($n_i > 0$) or removed from ($n_i < 0$) the defect-free crystal supercell; ε_F is the Fermi level (referenced to the valence-band maximum in the bulk, ε_V); ΔV is a factor that aligns the electrostatic potential to make the average potential in the defect-containing bulk the same as that in the defect-free bulk.

To determine the chemical potential of Li and H, we assume that there exist an equilibrium between the LiH , NH_3BH_3 and LiNH_2BH_3 , and thus the chemical potential of Li and H can be expressed as:

$$\mu_{\text{Li}} = \mu_{\text{LiNH}_2\text{BH}_3} - \mu_{\text{NH}_3\text{BH}_3} + \mu_{\text{H}} \quad (3)$$

$$\mu_{\text{H}} = \mu_{\text{LiH}} - \mu_{\text{Li}} \quad (4)$$

For the B and N related defects, the chemical potentials of BH_3 and NH_2 are referenced to the natural phase of diborane ($\mu_{\text{BH}_3} = \frac{1}{2}\mu_{\text{B}_2\text{H}_6}$) and ammonia ($\mu_{\text{NH}_2} = \mu_{\text{NH}_3} - \mu_{\text{H}}$).

3 Results and discussion

3.1 H related defects

The crystal structure of LiNH_2BH_3 is illustrated in Fig. 1, where the B–H and N–H bonds are drawn for clarity. The calculated lattice parameters of $a = 7.179$, $b = 14.196$ and $c = 5.253 \text{ \AA}$ are in

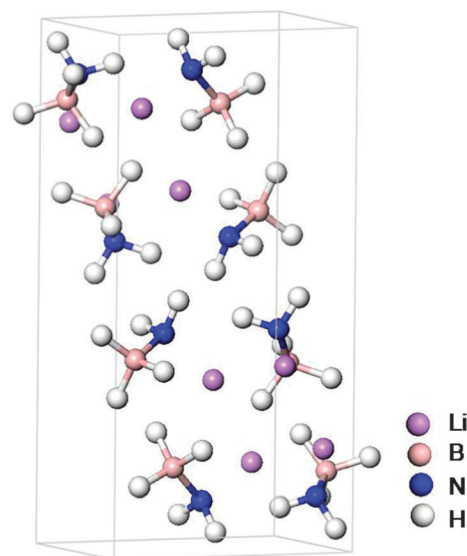


Fig. 1 The conventional unit cell of LiNH_2BH_3 .

good agreement with previous experimental and calculated results.^{4,24} The calculated band structure for LiNH_2BH_3 is shown in Fig. S1 (ESI[†]), which exhibits a large energy gap of about 4.1 eV, indicating that this compound is a wide-gap insulator. However, the band gaps of semiconductors and insulators are usually underestimated since density functional theory has difficulties in treating the excited states. The actual band gap of the LiNH_2BH_3 could be even larger. It has been reported that the excited states and band gaps can be further corrected by using the GW approximation.²⁹

For the H related defects in LiNH_2BH_3 , we first investigated atomic vacancies (V_{H}^q) and interstitials (I_{H}^q) in three possible charge states: $q = 0, -1$ and $+1$. Since LiNH_2BH_3 contains two groups of H atoms: (B)H and (N)H (Fig. 1), hydrogen vacancies were created in both cases. The notations $V_{(\text{B})\text{H}}^q$ and $V_{(\text{N})\text{H}}^q$ represent a vacancy on a B–H and N–H site with a net charge of q , respectively. In the case of I_{H}^q , we examined multiple possible initial positions to incorporate the H atom. In addition to the configuration of the H atom combined with a NH_2 to form a NH_3 unit, we also considered the configurations in which the H atom was put in the middle of the Li–N and Li–B bonds. Since previous DFT calculation works suggested that more complex aggregations of defects, *e.g.* divacancy and H_2 interstitials, could also contribute to H mobility in hydrogen storage materials,²¹ we also calculated the formation energies of divacancies (V_{H_2}) and H_2 interstitials (I_{H_2}) in LiNH_2BH_3 . The divacancy was created by directly removing the (N)H and (B)H atoms with the shortest dihydrogen bond in LiNH_2BH_3 . In the case of neutral I_{H_2} , a variety of possible configurations were examined.

The formation energies of hydrogen vacancies and interstitials for LiNH_2BH_3 as a function of the Fermi energy ε_{F} are plotted in Fig. 2. The lower limit for the Fermi level $\varepsilon_{\text{F}} = 0$ eV corresponds to the top of the valence band (VBM), while the upper limit $\varepsilon_{\text{F}} = 4.1$ eV represents the bottom of the conduction band (CBM). The vertical dashed line in Fig. 2 denotes the position of the relevant value of the Fermi energy which is found by determining the system with the lowest formation energy that is charge-neutral overall. Among the charge defects considered in this paper, the lowest formation energy is associated with V_{Li}^- and I_{Li}^+ with a formation energy of 0.50 eV. Thus, in the absence of extrinsic impurities, charge neutrality is achieved by equal concentrations of V_{Li}^- and I_{Li}^+ , which pins the Fermi level at ~ 2.34 eV. It can be seen from Fig. 2 that the major atomic H related defects are I_{H}^+ and I_{H}^- , with formation energies of 0.53 and 1.16 eV, respectively. The formation energy of I_{H}^0 is higher than either the positively or the negatively charged one for any value of the Fermi level. Hence, I_{H}^0 is unstable in equilibrium and will decay into a negatively charged state. The formation energy for $V_{(\text{B})\text{H}}^0$ is about 0.5 eV lower than that of $V_{(\text{N})\text{H}}^0$ in LiNH_2BH_3 . It can be explained by the fact that the bonding strength of N–H is stronger than that of B–H, which has also been reported by previous DFT works.^{27,37} The formation energy of $V_{(\text{N})\text{H}}^+$ is almost the same as $V_{(\text{B})\text{H}}^+$ due to the fact that the $V_{(\text{N})\text{H}}^+$ vacancy is unstable and would transform into the $V_{(\text{B})\text{H}}^+$ vacancy.

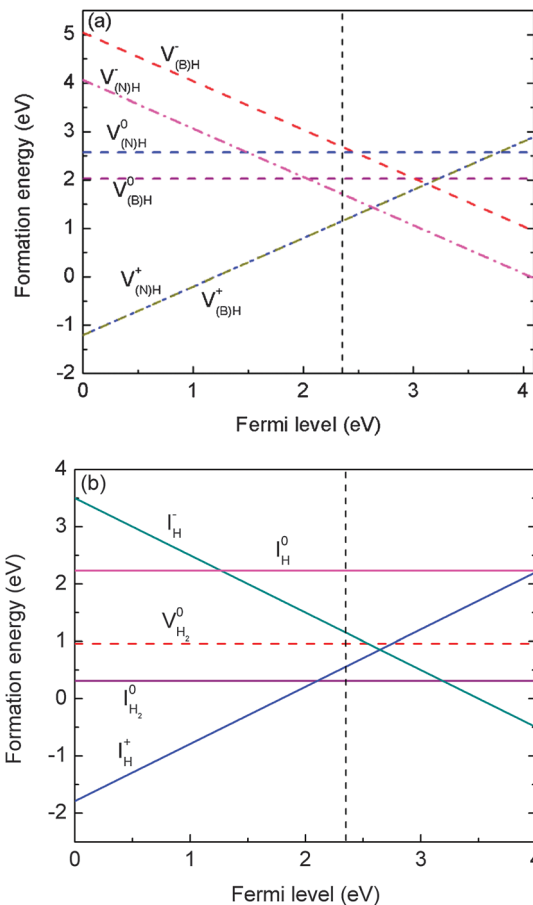


Fig. 2 The formation energies for H vacancies and interstitials as a function of the Fermi energy, ε_{F} .

It was reported that neutral H divacancies and neutral H_2 interstitials are the dominant defects in LiBH_4 due to their low formation energies. To consider the analogous situation for LiNH_2BH_3 , the formation energies for forming H divacancies and H_2 interstitials were examined. For the neutral H divacancy (V_{H_2}), the calculated formation energy is 1.0 eV, which is about 1.86 eV lower than the sum of formation energies of the isolated $V_{(\text{B})\text{H}}^+$ and $V_{(\text{N})\text{H}}^-$. Thus, the formation of the V_{H_2} is favored over the isolated $V_{(\text{B})\text{H}}^+$ and $V_{(\text{N})\text{H}}^-$. More importantly, it was found that the formation energy for the interstitial H_2 neutral is only 0.31 eV, which is lower than that of the isolated H vacancies and interstitials in all possible charge states. Additionally, the formation energy of H_2 interstitial in LiNH_2BH_3 is lower than the analogous result in LiBH_4 (0.42 eV). Therefore, according to eqn (1), the equilibrium concentration of neutral H_2 interstitials will be higher in LiNH_2BH_3 than in LiBH_4 . We further examined the enthalpy for forming a H_2 interstitial from isolated interstitials: $I_{\text{H}}^+ + I_{\text{H}}^- \rightarrow I_{\text{H}_2}$. This process has a net enthalpy of 1.38 eV. This huge enthalpy change favors the formation of a neutral H_2 interstitial relative to individual interstitials, implying that I_{H}^+ and I_{H}^- are present only in minute concentrations relative to the neutral H_2 interstitial.

Schematic representations of the relaxed local structures induced by H vacancies and interstitials are shown in Fig. 3.

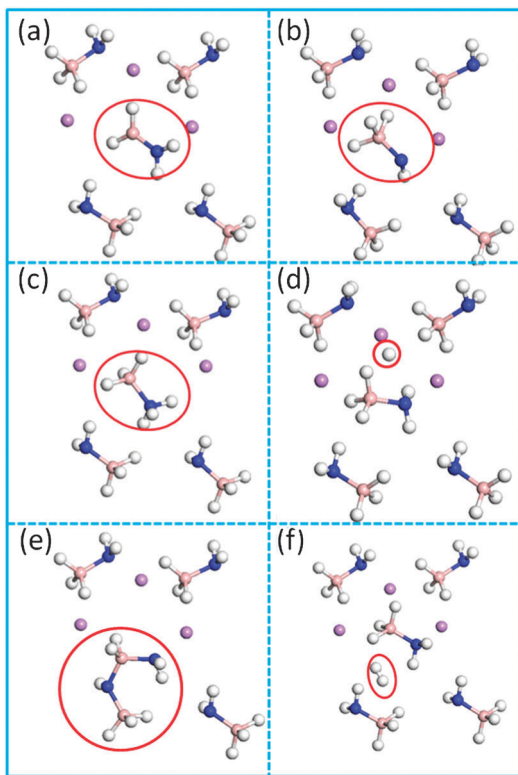


Fig. 3 Local structures induced by H related defects. (a) $V_{(B)H^+}$, (b) $V_{(N)H^-}$, (c) I_{H^+} , (d) I_{H^-} , (e) V_{H_2} and (f) I_{H_2} .

It shows that the B–N bond changes significantly due to the removal of a H atom from the BH_3/NH_3 unit. For example, the B–N bond length reduces from 1.546 to 1.392 Å for $V_{(B)H^+}$ vacancy. The calculated results also show a noticeable rotation of the B–H bonds toward the vacancy site of $V_{(B)H^+}$ (see in Fig. 2(a)). After creating the $V_{(N)H^-}$ vacancy, the B–N bond length reduces from 1.546 to 1.485 Å, accompanied with the rotation of N–H bonds toward the vacancy site (see in Fig. 2(b)).

For the positively charged H interstitial, I_{H^+} , the most stable configuration is achieved when the interstitial proton combines with a NH_2 unit to form a NH_3-BH_3 complex, as shown in Fig. 3(c). This can be explained by the Coulomb attraction between the extra H^+ cation and the $[NH_2]^-$ anion. In addition to the formation of NH_3 unit, the structure is further stabilized by stretching the nearest-neighbor Li–N distance from 1.793 Å to 3.642 Å. In the case of I_{H^-} , the extra H^- is stable between Li and NH_2 unit with the Li–H and H–H(N) distances of 1.747 and 1.923 Å, respectively.

The stable configuration of neutral H divacancy was obtained by rotating and moving the BH_2NH_2 complex close to the adjacent $NHBH_3$ complex until a new bridge N–B bond could be formed (see in Fig. 3(e)). The calculated formation energy of the neutral H divacancy is 0.96 eV, which is much lower than the sum of the formation energies of $V_{(B)H^+}$ and $V_{(N)H^-}$ (2.86 eV). The decreased formation energy of V_{H_2} can be attributed to the formation of the covalent B–N bond which strongly compensates for the energy increase due to the lattice

distortion, resulting in a relatively low formation energy compared to that of individual vacancies.

However, as shown in Fig. 3(f), the presence of the neutral H_2 interstitial molecule does not induce significant local lattice relaxations. The extra H_2 molecule is stable between two NH_2BH_3 units. The atomic distance of the H_2 molecule (0.756 Å) incorporated in the $LiNH_2BH_3$ lattice is still identical with the bond length of the free H_2 molecule.

3.2 Li related defects

The formation energies of vacancies and interstitials for the Li atom were calculated in three possible charge states: $q = +1, 0$ and -1 . For the Li vacancy (V_{Li}^q), a Li atom was directly removed from the $LiNH_2BH_3$ molecule. In the case of Li interstitials (I_{Li}^q), a variety of possible initial positions were considered to incorporate with the I_{Li}^q . In addition to locating the Li atom in the middle of the two NH_2 units, we also examined the configurations in which the Li atom was located between the NH_2 and BH_3 groups, and only the I_{Li}^q with the lowest formation energies were discussed in this paper.

The formation energies of various charged states for Li related defects as a function of the Fermi level are shown in Fig. 4. It shows that the Li vacancy is stable only in a negatively charged state (V_{Li}^-), and the formation energies of V_{Li}^0 and V_{Li}^+ are relatively high at any position of the Fermi level. Therefore, incorporation of V_{Li}^0 and V_{Li}^+ into the $LiNH_2BH_3$ lattice are unfavorable. For I_{Li}^q , it can be stable only in a positively charged state, which is energetically favorable over neutral and negatively charged states in the whole range of the band gap. I_{Li}^- shows the highest formation energy among the three types of Li interstitials in the entire band gap.

The local atomic relaxations around I_{Li}^+ and V_{Li}^- are shown in Fig. 5. After removing the Li^- , a noticeable rotation of the neighboring N–H bonds toward the vacancy site was observed. For the I_{Li}^+ interstitials, the extra Li cation sits in an arrangement between two $LiNH_2BH_3$ molecules with Li–H(B) distances of 1.948 and 2.005 Å, respectively.

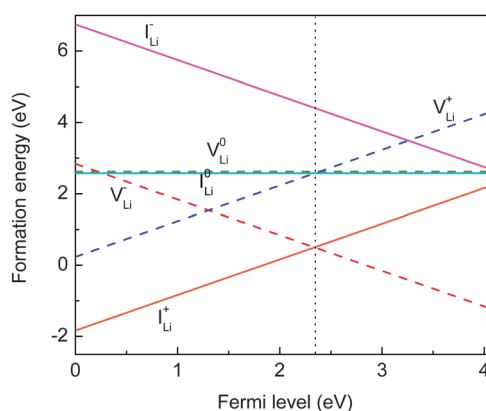


Fig. 4 The formation energies for Li vacancies and interstitials as a function of the Fermi energy, ϵ_F .

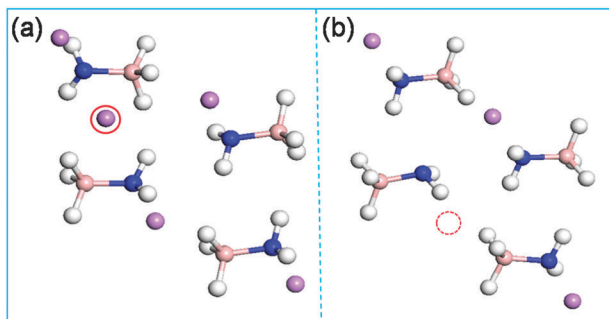


Fig. 5 Local structures induced by (a) I_{Li}^+ and (b) V_{Li}^- .

3.3 N and B related defects

The formation ability of NH_2 and BH_3 defects in $LiNH_2BH_3$ was further investigated. The NH_2/BH_3 vacancies were created by removing an NH_2 or BH_3 from one $LiNH_2BH_3$ molecule in the solid lithium amidoborane. The NH_2/BH_3 vacancies ($V_{NH_2}^q/V_{BH_3}^q$) and interstitial ($I_{NH_2}^q/I_{BH_3}^q$) in charged states from -1 to $+1$ were investigated. The calculated formation energies as a function of ϵ_F for these defects are shown in Fig. 6. Among the

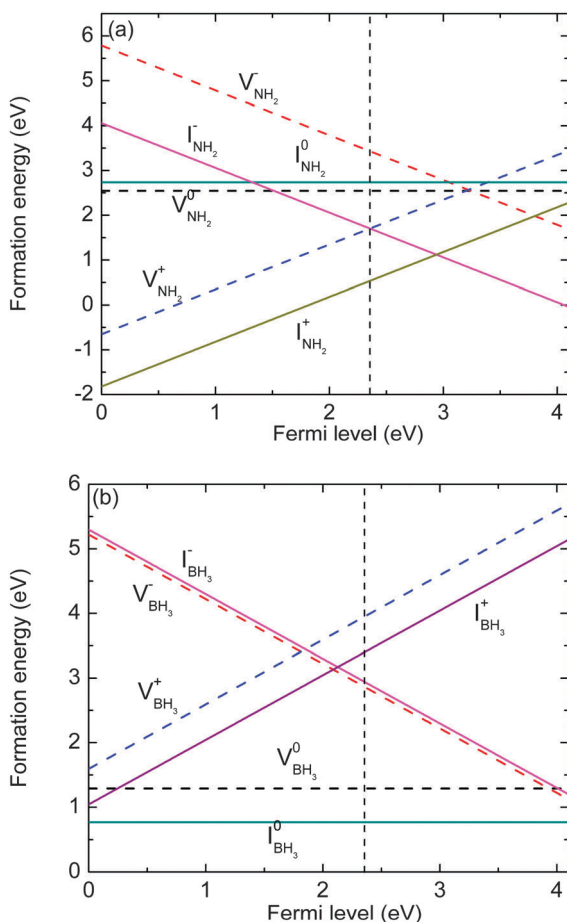


Fig. 6 The formation energies for (a) NH_2 and (b) BH_3 related defects as a function of the Fermi energy, ϵ_F .

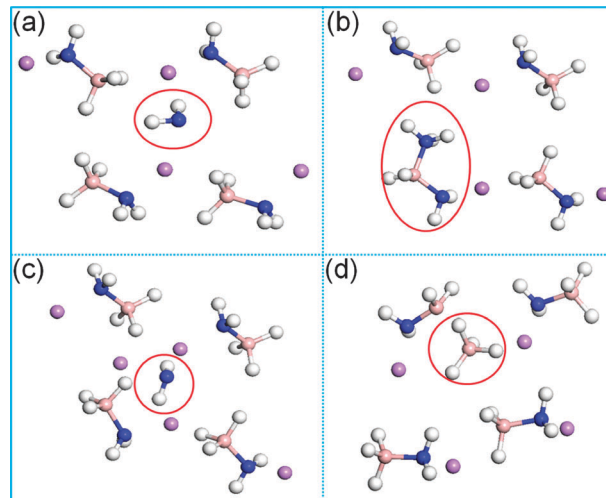


Fig. 7 Local structures induced by (a) $I_{NH_2}^+$, (b) $I_{NH_2}^-$, (c) $V_{BH_3}^0$ and (d) $I_{BH_3}^0$.

NH_2 related defects, negatively and positively charged NH_2 interstitials show the lowest formation energies over the entire range of Fermi level values. The neutral NH_2 vacancy and interstitial are high in energy, implying that these defects are not stable in equilibrium. In the case of the BH_3 defect, unlike the presence of charged NH_2 interstitial, the lowest-energy defect is $I_{BH_3}^0$ with the formation energy of 0.84 eV as shown in Fig. 6(b).

The lattice relaxations that occur around the NH_2 and BH_3 defects are illustrated in Fig. 7. The different charge states of the interstitial, $I_{NH_2}^+$ and $I_{NH_2}^-$ give rise to very different local lattice rearrangements. The introduction of $I_{NH_2}^-$ results in a H atom breaking away from a nearby BH_3 unit and forming a NH_3 interstitial. In addition, the NH_3 unit moves toward BH_2 until a new N-B bond is formed. In other words, $I_{NH_2}^-$ leads to the formation of a $NH_3-BH_2-NH_3$ complex. Upon the introduction of $I_{NH_2}^+$, the two nearest-neighbor BH_3NH_2 complexes significantly relax outward by $\sim 43\%$ of the B-B equilibrium distance. The extra NH_2 is stable in the interstitial site of the $LiNH_2BH_3$ lattice. The distances between the extra N and the two near Li atoms are 2.093 and 2.172 Å, respectively.

In the case of $V_{BH_3}^0$, the creation of a BH_3 vacancy leaves the system with an isolated NH_2 unit which moves toward the vicinity of Li cations due to the Coulombic attraction. Finally, this NH_2 unit is coordinated with three Li cations with Li-N distances of 2.016, 2.070 and 2.172 Å, respectively. The introduction of $I_{BH_3}^0$ results in a H atom breaking away from a nearby BH_3 unit (B-H bond stretches from 1.234 to 1.342 Å) and forming a bond with the BH_3 interstitial (with B-H bond length of 1.275 Å). In other words, the final geometry can be considered to consist of a hydrogen vacancy in the (B)H neutral charge defect, plus an interstitial BH_4 unit.

3.4 Diffusion barriers and activation energies

In addition to the formation energies of native defects and their effect on the local structures, we further investigated the

migration process of the H and Li related defects, which involves mass transport and is related to the dehydrogenation of LiNH_2BH_3 . Although numerous diffusion pathways in LiNH_2BH_3 were examined, only the lowest energy paths observed were described herein. For better understanding of the diffusion processes, documents which include the trajectories of these diffusion events were given in the ESI†

We first investigated the diffusion paths of hydrogen vacancies and interstitials in LiNH_2BH_3 and estimated the energy barriers for diffusion using the climbing image nudged elastic band (CI-NEB) method.³⁸ The migration barrier is defined as the energy difference between the saddle point and the ground state. For vacancies, the migration paths were calculated by moving a hydrogen atom from a nearby lattice site into the vacancy. The migration paths of interstitials were calculated by moving the extra hydrogen between ground state, *i.e.*, between two LiNH_2BH_3 molecules in the lattice.

The $V_{(\text{B})\text{H}}^+$ vacancy can be viewed as the removal of H^- from the BH_3 . We calculated the migration barrier for this defect by moving a H atom from a neighboring BH_3 unit into the vacancy. As shown in Fig. S2 (ESI†), the migration barrier of this defect is relatively high (0.61 eV). The concerted diffusion pathway for $V_{(\text{B})\text{H}}^+$ is shown in Fig. 8. The relatively high migration barrier for $V_{(\text{B})\text{H}}^+$ can be explained by the fact that this diffusion process involves two stages: first the rotation and stretching of the B–H and B–N bonds in the nearby LiNH_2BH_3 molecules, and then the breaking of one B–H bond and the formation of another.

The $V_{(\text{N})\text{H}}^-$ can be thought of as the extraction of a proton from the NH_2 unit, and the calculated migration barrier for this defect is only 0.29 eV (see in Fig. S2, ESI†). The saddle-point configuration of this defect consists of a hydrogen atom located midway between two NH_2BH_2 complexes with the H–N distances of 1.326 Å. Compared to the diffusion process of the $V_{(\text{B})\text{H}}^+$ vacancy, the diffusion of $V_{(\text{N})\text{H}}^-$ has a relatively small impact on the geometry (see Fig. 9).

The diffusion pathways of I_{H}^+ and I_{H}^- are shown in Fig. 10 and 11, respectively. The migration barrier for I_{H}^+ was calculated by moving a H atom from the NH_3 unit to the nearest NH_2 . The diffusion barrier of this process is 0.68 eV (see in Fig. S3, ESI†). In the case of I_{H}^- , the extra H^- moves from a H interstitial site to the nearby interstitial site. The saddle-point configuration in this case consists of a hydrogen atom located

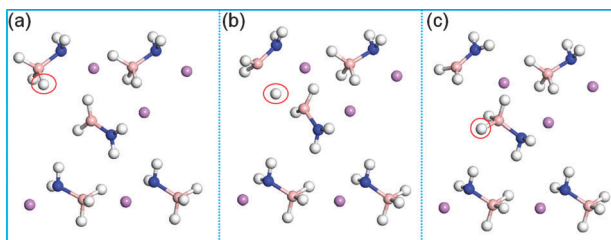


Fig. 8 Concerted diffusion pathway of $V_{(\text{B})\text{H}}^+$ vacancy in LiNH_2BH_3 . (a) Initial, (b) transition state and (c) final state.

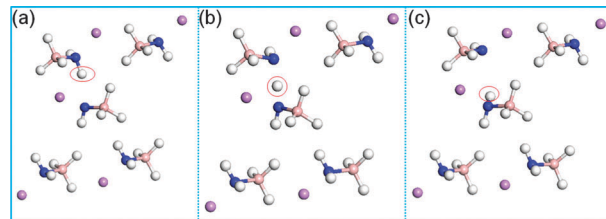


Fig. 9 Concerted diffusion pathway of $V_{(\text{N})\text{H}}^-$ vacancy in LiNH_2BH_3 . (a) Initial, (b) transition state and (c) final state.

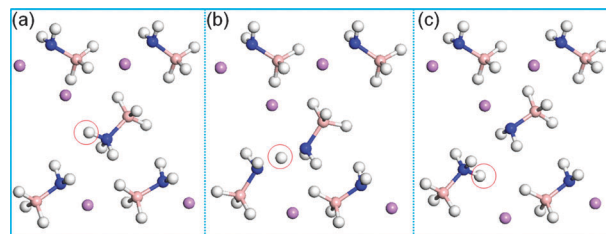


Fig. 10 Concerted diffusion pathway of I_{H}^+ interstitial in LiNH_2BH_3 . (a) Initial, (b) transition state and (c) final state.

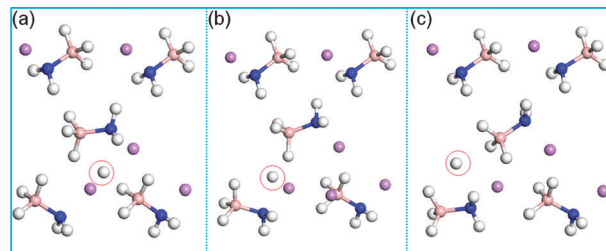


Fig. 11 Concerted diffusion pathway of I_{H}^- interstitial in LiNH_2BH_3 . (a) Initial, (b) transition state and (c) final state.

midway between two LiNH_2BH_3 molecules. As shown in Fig. S3 (ESI†), the migration barrier of I_{H}^+ was calculated to be 0.50 eV.

In the case of I_{H_2} , it was found that the extra H_2 could move from one interstitial site to another along the [001] direction with a low barrier of 0.16 eV, and the migration energy barrier for I_{H_2} along the [100] direction is 0.19 eV. The energy profiles for the two processes are shown in Fig. S4 (ESI†). The low migration barriers suggest that I_{H_2} could be mobile even at relatively low temperatures. The diffusion pathways of I_{H_2} along the [100] and [001] directions are shown in Fig. 12 and 13, respectively, which show that the bond length of the H_2 molecule is preserved along the migration path of I_{H_2} .

Next, the migration of Li related defects were characterized, which would be relevant to the transport of Li in LiNH_2BH_3 . The diffusion pathways of I_{Li}^+ and V_{Li}^- are shown in Fig. 14 and 15. The migration of I_{Li}^+ involves moving the Li^+ ion between two ground states, and the energy barrier of this process is 0.32 eV (see in Fig. S5, ESI†).

For V_{Li}^- , the migration involves moving Li^- from a nearby lattice site to the vacancy and this gives a relatively low energy

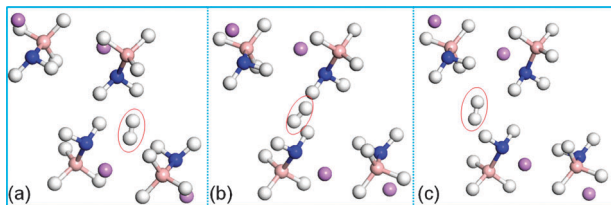


Fig. 12 Diffusion pathway of neutral H_2 interstitial along the $[100]$ direction. (a) Initial, (b) transition state and (c) final state.

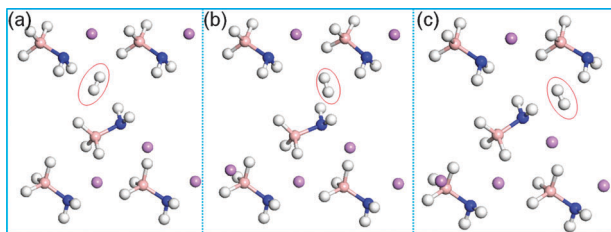


Fig. 13 Diffusion pathway of neutral H_2 interstitial along the $[001]$ direction. (a) Initial, (b) transition state and (c) final state.

barrier of 0.13 eV, indicating the high mobility of V_{Li}^- . As shown in Fig. 15 and Fig. S5 (ESI[†]), the Li^- first moves into the local minimum state (Fig. 15(c)) where the Li sites between two NH_2BH_3 complexes with Li–N distances of 2.065 and 2.179 Å. This migration process involves the movement of Li^- and the rotation of the nearby NH_2 toward the vacancy site. Starting from the local minimum state, the final configuration was achieved by rotating the NH_2 units opposite to the vacancy site.

The activation energy (E_a) for self-diffusion can be obtained by combining the calculated defect formation energy with the migration barrier. A summary for the activation energies of selective H and Li related defects is presented in Table 1. It is shown that I_{H_2} has the lowest activation energy (0.47 eV) for self-diffusion in all the defects considered above, indicating that I_{H_2} is the predominant diffusion species in $LiNH_2BH_3$. The low activation energy of I_{H_2} suggests that it can diffuse even at a relatively low temperature, resulting in fast kinetics for the dehydrogenation process of $LiNH_2BH_3$. On the other hand, $V_{(B)H}^+$ processes the highest activation energy (1.76 eV) due to its high formation energy and migration barrier (Table 1). In the case of $V_{(N)H}^-$, the formation energy is much higher than its migration barrier. Hence, according to eqn (1), the equilibrium concentration of $V_{(N)H}^-$ is low and the formation of $V_{(N)H}^-$ is

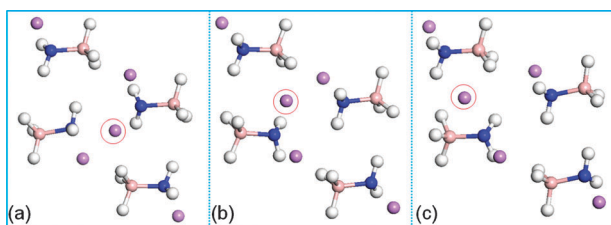


Fig. 14 Concerted diffusion pathway of I_{Li}^+ interstitial in $LiNH_2BH_3$. (a) Initial, (b) transition state and (c) final state.

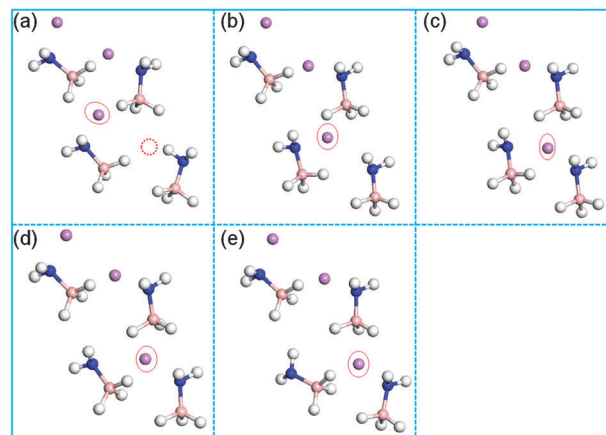


Fig. 15 Concerted diffusion pathway of V_{Li}^- vacancy in $LiNH_2BH_3$. (a) Initial, (b) transition state, (c) local minimum state, (d) transition state and (e) final state.

Table 1 Calculated defect formation energies (E_f), migration barriers (E_m) and activation energies ($Q = E_f + E_m$) for self-diffusion for selective defects in $LiNH_2BH_3$. Formation energies are taken at the position of the Fermi level

Defect	$V_{(B)H}^+$	$V_{(N)H}^-$	I_H^+	I_H^-	I_{H_2}	I_{Li}^+	V_{Li}^-
E_f	1.15	1.71	0.53	1.16	0.31	0.50	0.50
E_m	0.61	0.29	0.68	0.50	0.16	0.32	0.13
Q	1.76	2.0	1.21	1.66	0.47	0.82	0.63

the bottleneck for its transport. The activation energy for I_H^+ is 1.66 eV, which is about 0.45 eV higher than that of I_H^- . The calculated activation energies of V_{Li}^- and I_{Li}^+ are 0.63 and 0.82 eV, respectively. It should be noted that the formation energy for V_{Li}^- is slightly higher than its migration barrier, while the formation energy of I_{Li}^+ is about 0.37 eV higher than its migration barrier. The high formation energy of I_{Li}^+ would limit Li transport in $LiNH_2BH_3$ bulk.

The results above show that the diffusion of defects in $LiNH_2BH_3$ is very different from the situation in MgH_2 , $NaAlH_4$ and $LiNH_2$.^{16–20} In the latter materials, charged defects dominate H diffusion, while in $LiNH_2BH_3$, neutral H_2 interstitial is the relevant species. The previous DFT calculation results suggested that the H diffusion in $LiBH_4$, $NaBH_4$ and KBH_4 are dominated by motion of neutral H_2 interstitial molecules with activation energies of 0.66, 1.41 and 0.78 eV, respectively.²¹ However, the activation energy of neutral H_2 interstitial in $LiNH_2BH_3$ is significantly lower than that in these borohydrides, suggesting the high mobility of neutral H_2 interstitial in $LiNH_2BH_3$ compared to that in borohydrides. Therefore, the low activation energy of neutral H_2 interstitial probably contributes to the experimental observation of fast kinetics for the dehydrogenation process of $LiNH_2BH_3$ (with a dehydrogenation peak at 89 °C).⁴

It should be noted that the migration barriers of $V_{(N)H}^-$, V_{Li}^- and I_{Li}^+ are relatively low, indicating that the formation energies of these defects are the dominant terms in the activation energies for self-diffusion. The relatively high formation energies would result in the low concentration of $V_{(N)H}^-$, V_{Li}^-

and I_{Li}^+ defects, which limit their transport in bulk LiNH_2BH_3 . Since the formation energies of charged defects are Fermi level dependent, the formation energies of these point defects can be tuned by shifting the Fermi level, and then resulting in the improvement of the dehydrogenation kinetics of LiNH_2BH_3 . This can be achieved by adding appropriate impurities that are electrically active into the systems.

4 Conclusions

In summary, native defects in LiNH_2BH_3 were studied using first-principles calculations. Defect-induced local structures and defect formation energies of H, Li, B and N related vacancies and interstitials in various charged states were examined. The energetically favorable atomic H defects are positively and negatively charged H interstitials (I_{H}^+ and I_{H}^-). The Li related defects are dominated by a positively charged Li interstitial (I_{Li}^+) and a negatively charged Li vacancy (V_{Li}^-). For N related defects, positively and negatively charged NH_2 interstitials ($I_{\text{NH}_2}^+$ and $I_{\text{NH}_2}^-$) have the lowest formation energies. In the case of B related defects, the lowest-energy defect is neutral BH_3 interstitial ($I_{\text{BH}_3}^0$). Furthermore, the formation energy of neutral H_2 interstitial (I_{H_2}) is as low as 0.31 eV, indicating that the dominant defects in LiNH_2BH_3 are neutral H_2 interstitial rather than the charge defects associated with the individual H and Li atoms or B/N related defects. Investigation of the migration of H and Li related defects in several possible diffusion pathways indicated that the migration barriers for $V_{(\text{B})\text{H}}^+$ (positively charged H vacancy on a B–H site), I_{H}^+ and I_{H}^- are relatively high (0.50–0.68 eV), whereas moderate diffusion barriers are presented for $V_{(\text{N})\text{H}}^-$ (the negatively charged H vacancy on a N–H site) and I_{Li}^+ (0.29 and 0.32 eV, respectively). The migration barriers for V_{Li}^- and I_{H_2} defects are calculated to be 0.13 and 0.16 eV, respectively. With a low activation energy of 0.47 eV, I_{H_2} is the major diffusive species in LiNH_2BH_3 . Our calculation results further suggest that the creation of the $V_{(\text{N})\text{H}}^-$, I_{Li}^+ and V_{Li}^- defects is the rate-limiting step for their transportation in LiNH_2BH_3 .

Acknowledgements

This work was partially supported by the Ministry of Science and Technology of China (2010CB631302), the National Natural Science Foundation of China (Grant No. 51071047, 21271046), the PhD Programs Foundation of Ministry of Education of China (201110071110009) and the Science and Technology Commission of Shanghai Municipality (11JC1400700, 11520701100).

References

- 1 W. Grochala and P. P. Edwards, *Chem. Rev.*, 2004, **104**, 1283–1316.
- 2 L. Schlapbach and A. Züttel, *Nature*, 2001, **414**, 353–358.
- 3 S. Orimo, Y. Nakamori, J. R. Eliseo, A. Züttel and C. M. Jensen, *Chem. Rev.*, 2007, **107**, 4111–4132.

- 4 Z. Xiong, C. K. Yong, G. Wu, P. Chen, W. Shaw, A. Karkamkar, T. Autrey, M. O. Jones, S. R. Johnson and P. P. Edwards, *Nat. Mater.*, 2008, **7**, 138–141.
- 5 T. B. Marder, *Angew. Chem., Int. Ed.*, 2007, **46**, 8116–8118.
- 6 A. Staubitz, A. P. M. Robertson and I. Manners, *Chem. Rev.*, 2010, **110**, 4079–4124.
- 7 C. W. Hamilton, R. T. Baker, A. Staubitz and I. Manners, *Chem. Soc. Rev.*, 2009, **38**, 279–293.
- 8 X. Kang, Z. Fang, L. Kong, H. Cheng, X. Yao, G. Lu and P. Wang, *Adv. Mater.*, 2008, **20**, 2756–2759.
- 9 A. T. Luedtke and T. Autrey, *Inorg. Chem.*, 2010, **49**, 3905–3910.
- 10 H. Wu, W. Zhou and T. Yildirim, *J. Am. Chem. Soc.*, 2008, **130**, 14834–14839.
- 11 H. V. K. Diyabalanage, R. P. Shrestha, T. A. Semelsberger, B. L. Scott, M. E. Bowden, B. L. Davis and A. K. Burrell, *Angew. Chem., Int. Ed.*, 2007, **46**, 8995–8997.
- 12 H. Wu, W. Zhou, F. E. Pinkerton, M. S. Meyer, Q. Yao, S. Gadipelli, T. J. Udovic, T. Yildirim and J. J. Rush, *Chem. Commun.*, 2011, **47**, 4102–4104.
- 13 K. J. Fijalkowski, R. V. Genova, Y. Filinchuk, A. Budzianowski, M. Derzsi, T. Jaroń, P. J. Leszczyński and W. Grochala, *Dalton Trans.*, 2011, **40**, 4407.
- 14 F. A. Kröger and N. H. Nachtrieb, *Phys. Today*, 1964, **17**, 66.
- 15 A. Peles and C. G. Van de Walle, *Phys. Rev. B: Condens. Matter Mater. Phys.*, 2007, **76**, 214101.
- 16 G. B. Wilson-Short, A. Janotti, K. Hoang, A. Peles and C. G. Van de Walle, *Phys. Rev. B: Condens. Matter Mater. Phys.*, 2009, **80**, 224102.
- 17 M. S. Park, A. Janotti and C. G. Van de Walle, *Phys. Rev. B: Condens. Matter Mater. Phys.*, 2009, **80**, 064102.
- 18 S. Hao and D. S. Sholl, *Appl. Phys. Lett.*, 2008, **93**, 251901.
- 19 J. Wang, Y. Du, H. Xu, C. Jiang, Y. Kong, L. Sun and Z. K. Liu, *Phys. Rev. B: Condens. Matter Mater. Phys.*, 2011, **84**, 024107.
- 20 E. Hazrati, G. Brocks, B. Buurman, R. de Groot and G. de Wijs, *Phys. Chem. Chem. Phys.*, 2011, **13**, 6043–6052.
- 21 S. Hao and D. S. Sholl, *Phys. Chem. Chem. Phys.*, 2009, **11**, 11106–11109.
- 22 D. West, S. Limpijumngong and S. B. Zhang, *Phys. Rev. B: Condens. Matter Mater. Phys.*, 2009, **80**, 064109.
- 23 D. Y. Kim, H. M. Lee and K. S. Kim, *Chem.–Eur. J.*, 2009, **15**, 5598–5604.
- 24 S. M. Lee, X. D. Kang, P. Wang, H. M. Cheng and Y. H. Lee, *ChemPhysChem*, 2009, **10**, 1825–1833.
- 25 T. B. Lee and M. L. McKee, *Inorg. Chem.*, 2009, **48**, 7564–7575.
- 26 P. M. Zimmerman, A. Paul, Z. Zhang and C. B. Musgrave, *Inorg. Chem.*, 2009, **48**, 1069–1081.
- 27 W. Li, R. H. Scheicher, C. M. Araujo, G. Wu, A. Blomqvist, C. Wu, R. Ahuja, Y. P. Feng and P. Chen, *J. Phys. Chem. C*, 2010, **114**, 19089–19095.
- 28 C. Bheema Lingam, K. R. Babu, S. P. Tewari and G. J. Vaitheeswaran, *J. Comput. Chem.*, 2012, **33**, 987–997.
- 29 C. Bheema Lingam, K. Ramesh Babu, S. P. Tewari, G. Vaitheeswaran and S. J. Lebegue, *J. Phys. Chem. C*, 2011, **115**, 18795–18801.
- 30 J. P. Perdew, K. Burke and Y. Wang, *Phys. Rev. B: Condens. Matter*, 1996, **54**, 16533–16539.
- 31 P. E. Blöchl, *Phys. Rev. B: Condens. Matter*, 1994, **50**, 17953.
- 32 G. Kresse and J. Furthmüller, *Phys. Rev. B: Condens. Matter*, 1996, **54**, 11169.
- 33 G. Kresse and J. Hafner, *Phys. Rev. B: Condens. Matter*, 1993, **47**, 558–561.
- 34 H. J. Monkhorst and J. D. Pack, *Phys. Rev. B: Solid State*, 1976, **13**, 5188.
- 35 C. G. Van de Walle and J. J. Neugebauer, *J. Appl. Phys.*, 2004, **95**, 3851.
- 36 K. Matsunaga, T. Tanaka, T. Yamamoto and Y. Ikuhara, *Phys. Rev. B: Condens. Matter*, 2003, **68**, 085110.
- 37 M. Ramzan, F. Silvearv, A. Blomqvist, R. H. Scheicher, S. Lebegue and R. Ahuja, *Phys. Rev. B: Condens. Matter Mater. Phys.*, 2009, **79**, 132102.
- 38 G. Henkelman, B. P. Uberuaga and H. Jónsson, *J. Chem. Phys.*, 2000, **113**, 9901.